81–136, Macmillan, New York.
Patel, D. J., Kozlowski, S. A., Marky, L. A., Broka, C., Rice, J. A., Itakura, K., & Breslauer, K. J. (1982c) *Biochemistry 21*, 428–436.
Patel, D. J., Kozlowski, S. A., Nordheim, A., & Rich, A. (1983) *Proc. Natl. Acad. Sci. U.S.A. 79*, 1413–1417.
Patel, D. J., Shapiro, L., Kozlowski, S. A., Gaffney, B. L., & Jones, R. A. (1986) *Biochemistry* (following paper in this issue).
Redfield, A. G., Kunz, S. D., & Ralph, E. K. (1975) *J. Magn. Reson. 19*, 114–117.
Scheek, R. M., Boelens, R., Russo, N., van Boom, J. H., & Kaptein, R. (1984) *Biochemistry 23*, 1371–1376.
Singer, B. (1979) *JNCI, J. Natl. Cancer Inst. 62*, 1329–1339.
Singer, B., & Grunberger, D. (1983) in *Molecular Biology of Mutagens and Carcinogens*, Plenum, New York.
States, D. J., Haberkorn, R. A., & Ruben, D. J. (1982) *J. Magn. Reson. 48*, 286–292.
Weiss, M., Patel, D. J., Sauer, R. T., & Karplus, M. (1984a) *Proc. Natl. Acad. Sci. U.S.A. 81*, 130–134.
Weiss, M., Patel, D. J., Sauer, R. T., & Karplus, M. (1984b) *Nucleic Acids Res. 12*, 4035–4047.

Structural Studies of the O^{6}meG·T Interaction in the d(C-G-T-G-A-A-T-T-C-O^{6}meG-C-G) Duplex†

Dinshaw J. Patel* and Lawrence Shapiro
Department of Biochemistry and Molecular Biophysics, College of Physicians and Surgeons, Columbia University, New York, New York 10032
Sharon A. Kozlowski
Polymer Chemistry Department, AT&T Bell Laboratories, Murray Hill, New Jersey 07994
Barbara L. Gaffney and Roger A. Jones
Department of Chemistry, Rutgers, The State University of New Jersey, New Brunswick, New Jersey 08903
Received July 16, 1985

ABSTRACT: High-resolution proton and phosphorus NMR studies are reported on the self-complementary d(C_1-G_2-T_3-G_4-A_5-A_6-T_7-T_8-C_9-O^{6}meG$_{10}$-C_{11}-G_{12}) duplex (henceforth called O^{6}meG·T 12-mer), which contains T3·O^{6}meG10 interactions in the interior of the helix. The imino proton of T3 is observed at 9.0 ppm, exhibits a temperature-independent chemical shift in the premelting transition range, and broadens out at the same temperature as the imino proton of the adjacent G2·C11 toward the end of the helix at pH 6.8. We observed inter base pair nuclear Overhauser effects (NOEs) between the base protons at the T3·O^{6}meG10 modification site and the protons of flanking G2·C11 and G4·C9 base pairs, indicative of the stacking of the T3 and O^{6}meG10 bases into the helix. Two-dimensional correlated (COSY) and nuclear Overhauser effect (NOESY) studies have permitted assignment of the base and sugar H1′, H2′, and H2″ nonexchangeable protons in the O^{6}meG·T 12-mer duplex. The observed NOEs demonstrate an anti conformation about all the glycosidic bonds, and their directionality supports formation of a right-handed helix in solution. The observed NOEs between the T3·O^{6}meG10 interaction and the adjacent G2·C11 and G4·C9 base pairs at the modification site exhibit small departures from patterns for a regular helix in the O^{6}meG·T 12-mer duplex. The phosphorus resonances exhibit a 0.5 ppm spectral dispersion indicative of an unperturbed phosphodiester backbone for the O^{6}meG·T 12-mer duplex. We propose a model for pairing of T3 and O^{6}meG10 at the modification site in the O^{6}meG·T 12-mer duplex. This study compares the NMR parameters of the O^{6}meG·T 12-mer duplex with those of the G·T 12-mer duplex, which contains a T3·G10 mismatch at the same site in the helix.

The mutagenic and carcinogenic lesion resulting from the O^6-alkylation of guanosine (O^{6}meG) has been the focus of extensive biological studies to elucidate the consequences of this simple covalent modification of DNA. These studies include the base pairing properties of O^{6}meG in template DNA during in vitro replication (Snow et al., 1984) and in vivo mutagenesis studies following site-specific incorporation of O^{6}meG in viral genomes (Green et al., 1984; Loechler et al., 1984). The latter studies demonstrated that O^{6}meG induced exclusively G → A transitions indicative of O^{6}meG·T pairing in the viral genome.

Chart I

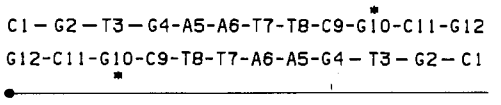

It has also been shown that the conversion of normal genes to oncogenes can result from G → A transition errors (Santos et al., 1983) and also from G → T transversion errors at a single G residue in the *ras* system (Tabin et al., 1982; Reddy

† This research was supported by National Institutes of Health Grant 1R01 GM34504 to D.J.P. and by American Cancer Society Grant CH-248 and National Institutes of Health Grant GM31483 to R.A.J. L.S. was supported by Biochemical Research Support Grant SO7RR05359-23.

0006-2960/86/0425-1036$01.50/0

et al., 1982; Taparowsky et al., 1982).

There is no structural information on the nature of the helix disruption resulting from the alkylation of guanosine in the interior of the helix. We have recently shown NMR to be a powerful spectroscopic tool to monitor the structure and dynamics at and adjacent to the mismatch and extra helical base sites in specially designed and synthesized DNA fragments (Patel et al., 1982a). We have therefore undertaken a systematic NMR study of O^{6}meG containing dodecanucleotides recently synthesized by Gaffney et al. (1984), who found that O^{6}meG incorporation creates a region of localized instability in the double helix.

We report below on the d(C_1-G_2-T_3-G_4-A_5-A_6-T_7-T_8-C_9-O^{6}meG$_{10}$-C_{11}-G_{12}) duplex (henceforth called O^{6}meG·T 12-mer duplex), which contains symmetrically related O^{6}meG·T interactions (Chart I). We have previously reported on the G·T mismatch pair in the d(C-G-T-G-A-A-T-T-C-G-C-G) duplex (henceforth called G·T 12-mer; Patel et al., 1982b), and this permits a comparison of the NMR structural parameters for the G·T 12-mer and O^{6}meG·T 12-mer duplexes in aqueous solution.

We also compare the NMR parameters for the O^{6}meG·C 12-mer [previous paper, Patel et al. (1986)] with the O^{6}meG·T 12-mer to evaluate the consequences of the introduction of C and T residues opposite the modified O^{6}meG base in the interior of the helix. Our NMR studies on the O^{6}meG·A 12-mer and the O^{6}meG·G 12-mer containing A and G residues opposite the O^{6}meG base will be reported elsewhere.

Experimental Procedures

The synthesis, purification, and analysis of the d(C-G-T-G-A-A-T-T-C-O^{6}meG-C-G) self-complementary dodecanucleotide duplex have been reported previously (Gaffney et al., 1984). The NMR sample was prepared on 150 A_{260} units of the O^{6}meG·T 12-mer duplex in 0.4 mL of 0.1 M NaCl, 10 mM phosphate, and 1 mM ethylenediaminetetraacetic acid (EDTA) buffer. The proton spectrum in H_2O and D_2O indicated a sample purity of >97%. The collection of one-dimensional proton spectra in H_2O and two-dimensional COSY and NOESY spectra in D_2O and data processing for the O^{6}meG·T 12-mer duplex were the same as reported in the accompanying paper on the O^{6}meG·C 12-mer duplex (Patel et al., 1986).

Results

The numbering system in the O^{6}meG·T 12-mer is designated in Chart I with the modification at the T3·O^{6}meG10 position.

Exchangeable Proton Assignments. The proton NMR spectrum of the O^{6}meG·T 12-mer duplex in 0.1 M NaCl, 10 mM phosphate, and H_2O, pH 6.8 at −5 °C, is presented in Figure 1A. The five Watson–Crick imino protons give well-resolved resonances between 12 and 14 ppm and can be assigned from the temperature dependence of their line widths and one-dimensional NOE measurements.

We observe sequential broadening of the 13.12 and 12.93 ppm imino protons on raising the temperature to 15 and 35 °C, respectively (Figure 2), permitting assignment to the imino protons of C1·G12 and G2·C11, respectively, due to fraying at the ends of the helix. The remaining guanosine imino proton at 12.30 ppm is assigned to G4·C9 while the two lowest field 13.84 and 13.75 ppm imino protons are assigned to the central A·T base pairs in the O^{6}meG·T 12-mer duplex at −5 °C (Figure 2). We observe an exchangeable proton at 9.05 ppm in the spectrum of the O^{6}meG·T 12-mer duplex, pH 6.8 at −5 °C (Figure 1), which is assigned to the imino proton of T3 in the T3·O^{6}meG10 interaction site.

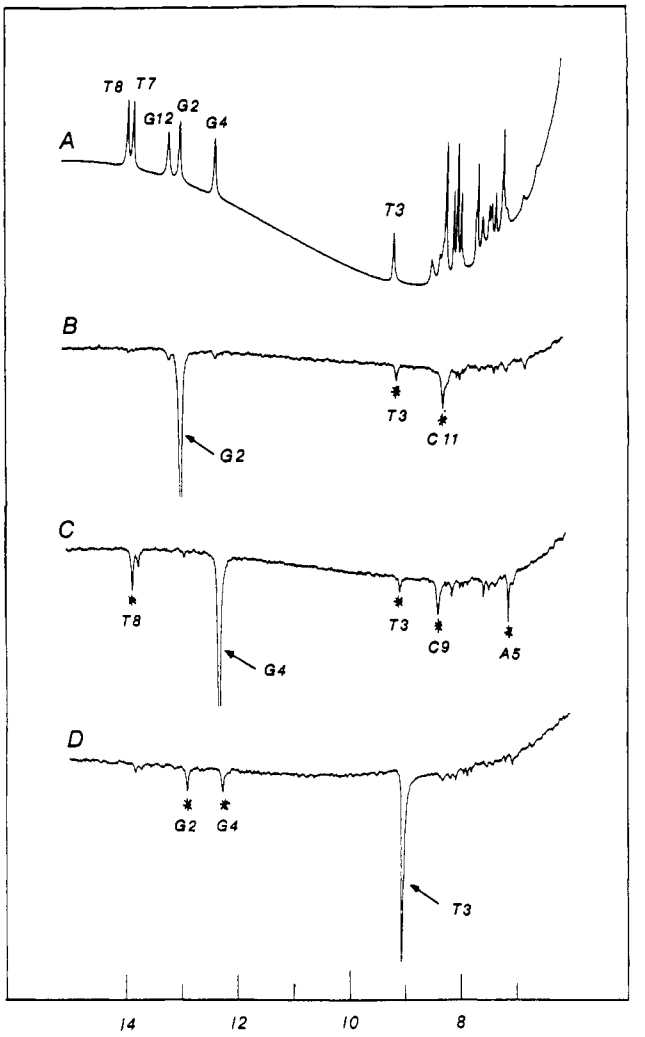

FIGURE 1: (A) 500-MHz proton NMR spectrum (6–15 ppm) of the O^{6}meG·T 12-mer in 0.1 M NaCl, 10 mM phosphate, and 1 mM EDTA in H_2O, pH 6.80 at −5 °C. Difference spectra following 1-s saturation of (B) the 12.93 ppm guanosine imino proton, (C) the 12.30 ppm guanosine imino proton, and (D) the 9.05 ppm thymidine imino proton. Saturation power levels resulted in ~50% saturation of the desired resonance. The saturated resonance is designated by an arrow while the observed NOEs are designated by asterisks.

We have undertaken one-dimensional NOEs (1-s saturation) on the imino protons of the O^{6}meG·T 12-mer duplex at −5 °C to determine whether the T3 and O^{6}meG10 bases are stacked into the duplex at the modification site. Saturation of the 12.93 ppm imino proton of G2·C11 results in an intra base pair NOE at the 8.22 ppm hydrogen-bonded cytidine amino proton and an inter base pair NOE at the 9.05 ppm imino proton of the adjacent T3·O^{6}meG10 interaction (Figure 1B). Saturation of the 12.30 ppm imino proton of G4·C9 results in an intra base pair NOE at the 8.36 ppm hydrogen-bonded cytidine amino proton and inter base NOEs at the 13.84 ppm imino and 7.11 ppm adenosine H2 proton of the adjacent A5·T8 base pair and the 9.05 ppm imino proton of the adjacent T3·O^{6}meG10 interaction (Figure 1C). We also detect weaker NOEs to protons on next-nearest-neighbor base pairs due to spin diffusion for 1-s saturation times at low temperature. Saturation of the 9.05 ppm imino proton of the T3·O^{6}meG10 interaction results in inter base pair NOEs at the 12.93 ppm imino proton of the adjacent G2·C11 base pair and 12.30 ppm of the adjacent G4·C9 base pair (Figure 1D). These NOE measurements demonstrate that T3 stacks into the helix and overlaps with the G2·C11 and G4·C9 base pairs in the O^{6}meG·T 12-mer duplex in solution. The imino, cytidine

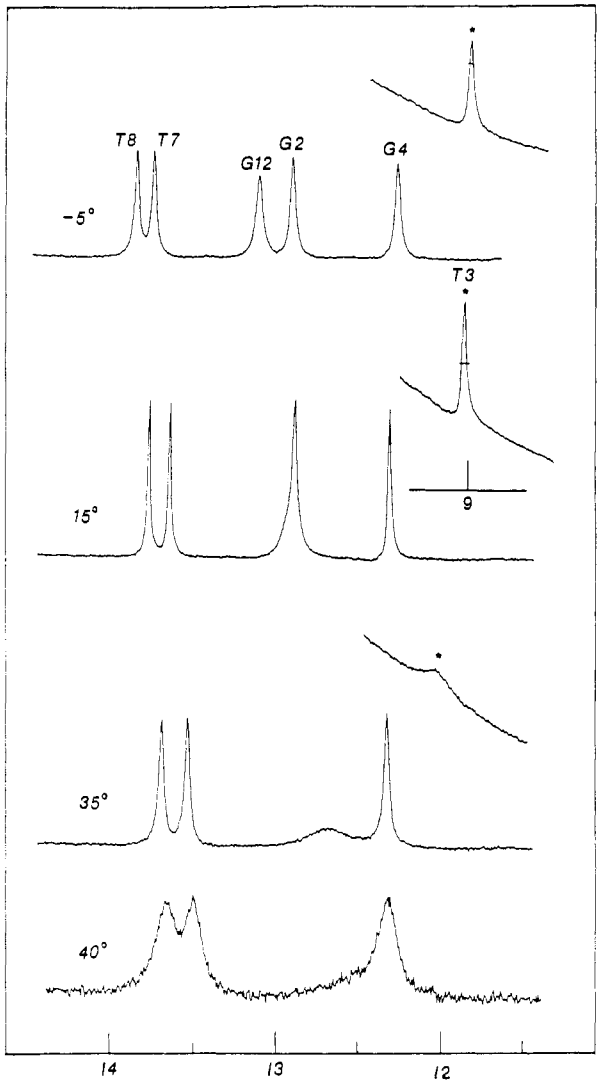

FIGURE 2: 500-MHz proton NMR spectra (12.5–14.5 ppm; 8.5–9.5 ppm) of the imino proton chemical shifts of the O⁶meG·T 12-mer in 0.1 M NaCl, 10 mM phosphate, and H_2O, pH 6.8, as a function of temperature between −5 and 40 °C. The imino proton assignments are designated over the resonances.

Table I: Proton Chemical Shifts of the Thymidine Imino, Guanosine Imino, Cytidine Amino, and Adenosine H2 Protons in the O⁶meG·T 12-mer at −5 °C[a]

pair	T H3	G H1	C H4	A H2
C1·G12		13.12	8.16	
G2·C11		12.93	8.22	
T3·O⁶meG10	9.05			
G4·C9		12.30	8.36	
A5·T8	13.84			7.11
A6·T7	13.75			7.56

[a] Buffer is 0.1 M NaCl, 10 mM phosphate, 1 mM EDTA, and H_2O, pH 6.8. [b] Chemical shift represents hydrogen-bonded cytidine amino protons.

amino, and adenosine H2 assignments of the O⁶meG·T 12-mer duplex at −5 °C are listed in Table I.

The temperature dependence of the line widths of the imino protons of the O⁶meG·T 12-mer duplex in 0.1 M NaCl and 10 mM phosphate, pH 6.8, is shown in Figure 2. We note that the imino protons of the G2·C11 base pair and the T3·O⁶meG10 interaction exhibit similar line-broadening changes with increasing temperature while the imino protons of G4·C9, A5·T8, and A6·T7 broaden simultaneously at somewhat higher temperatures (Figure 2).

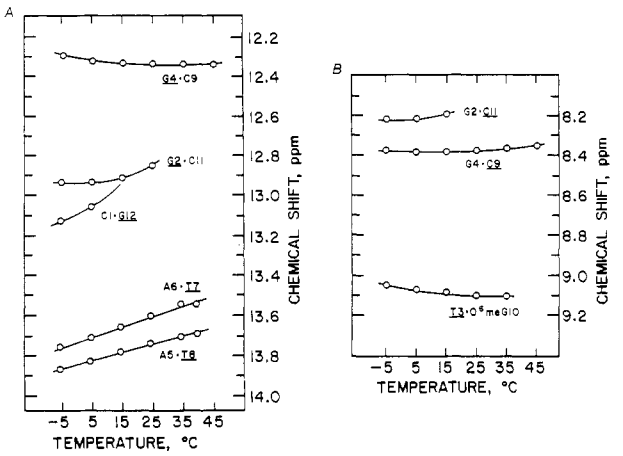

FIGURE 3: Temperature dependence of the imino and amino proton chemical shifts of the O⁶meG·T 12-mer in 0.1 M NaCl, 10 mM phosphate, 1 mm EDTA, and H_2O, pH 6.8, as a function of temperature between −5 and 40 °C. The imino and amino assignments are designated over the resonances.

The temperature dependence of the Watson–Crick imino (12–14 ppm) and the T3·O⁶meG10 imino and hydrogen-bonded cytidine amino proton chemical shifts in the O⁶meG·T 12-mer duplex is plotted in Figure 3. We note that the imino proton of the T3·O⁶meG10 interaction exhibits a temperature-independent chemical shift (Figure 3B) in contrast to the upfield shifts observed for the thymidine imino protons of A5·T8 and A6·T7 base pairs with increasing temperature (Figure 3A) in the O⁶meG·T 12-mer duplex.

Two-Dimensional Spectra of Nonexchangeable Protons. The nonexchangeable proton spectrum of the O⁶meG·T 12-mer in 0.1 M NaCl at 25 °C exhibits well-resolved base and sugar proton resonances with the OCH_3 group of O⁶meG10 resonating as a resolved peak at 3.74 ppm.

The magnitude COSY spectrum and the phase-sensitive NOESY spectrum of the O⁶meG·T 12-mer (nonspin) in 0.1 M NaCl have been recorded at 25 °C. The resolution and intensity of the cross peaks deteriorate close to the HOD resonance so that there is some uncertainty regarding spectral assignments in the sugar H3′, H4′, H5′, and H5″ region. We present the results below which establish the base and sugar H1′, H2′, and H2″ assignments on the basis of an analysis of the COSY and NOESY data sets.

Base to H1′ Connectivities. The expanded 250-ms mixing time NOESY contour plot of the base (7.0–8.2 ppm) and the sugar H1′ (5.2–6.2 ppm) protons in the O⁶meG·T 12-mer at 25 °C is shown in Figure 4. We have been able to trace the NOE connectivities between the base (purine H8 and pyrimidine H6) and their own and 5′-linked sugar H1′ protons characteristic of a right-handed helix. The resonances are resolved in both dimensions except that the H1′ protons of T3 and C9 are superimposed on each other (Figure 4).

The H8 of O⁶meG10 and the H6 of T3 at the T3·O⁶meG10 modification site exhibit NOEs to their own and 5′-flanked sugars characteristic of an unperturbed right-handed helix. The strongest cross peaks reflect the NOEs between the H5 and H6 protons (interproton distance of 2.4 Å) of C1, C9, and C11 (designated by asterisks in Figure 4) while the base to H1′ cross peaks exhibit much weaker intensities indicative of anti glycosidic torsion angles (interproton distance 3.7 Å). The base and sugar H1′ proton chemical shifts in the O⁶meG·T 12-mer in D_2O at 25 °C are listed in Table II.

Base to Base NOEs. We also detect NOEs amongst the base protons characteristic of a right-handed helix for the O⁶meG·T 12-mer duplex. Thus, NOEs are observed between

Table II: Base and Sugar Proton Chemical Shifts in the d(C-G-T-G-A-A-T-T-C-O^{6}meG-C-G) Duplex in 0.1 M NaCl, 10 mM Phosphate, and D_2O at 5 °C

	base				sugar		
	H8	H2	H6	H5/CH_3	H1′	H2′	H2″
C1			7.57	5.86	5.77	1.87	2.34
G2	7.89				5.98	2.63	2.63
T3			7.21	1.64	5.67	2.07	2.35
G4	7.81				5.43	2.60	2.69
A5	8.11	7.21			6.00	2.69	2.92
A6	8.09	7.57			6.13	2.58	2.88
T7			7.08	1.25	5.87	1.96	2.54
T8			7.35	1.51	6.06	2.11	2.52
C9			7.46	5.63	5.67	2.05	2.42
O^{6}meG10	7.97				5.89	2.60	2.60
C11			7.29	5.31	5.75	1.83	2.27
G12	7.92				6.14	2.60	2.35

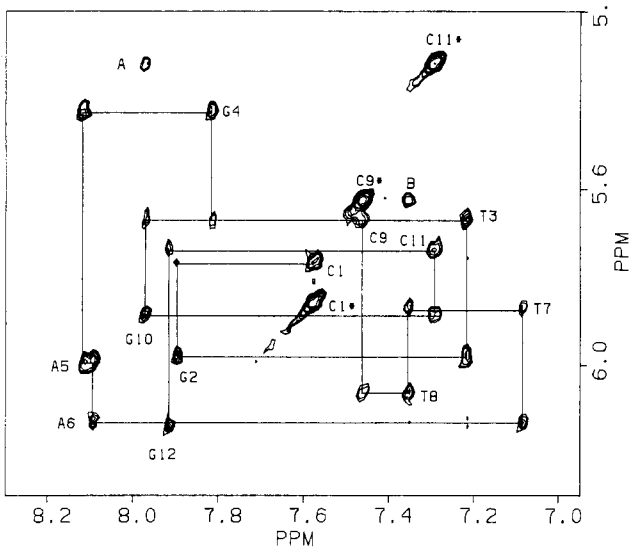

FIGURE 4: Expanded contour plot of the phase-sensitive NOESY spectrum (mixing time 250 ms) of the O^{6}meG·T 12-mer at 25 °C establishing distance connectivities between the base protons (7.0–8.2 ppm) and the sugar H1′ protons (5.2–6.3 ppm). The base and sugar H1′ assignments are depicted next to the contour peaks while additional cross peaks designated by A and B are discussed and assigned in the text. The asterisks designate the cytidine H5 to H6 connectivities. The lines follow the connectivities between the adjacent base protons through the intervening sugar H1′ protons.

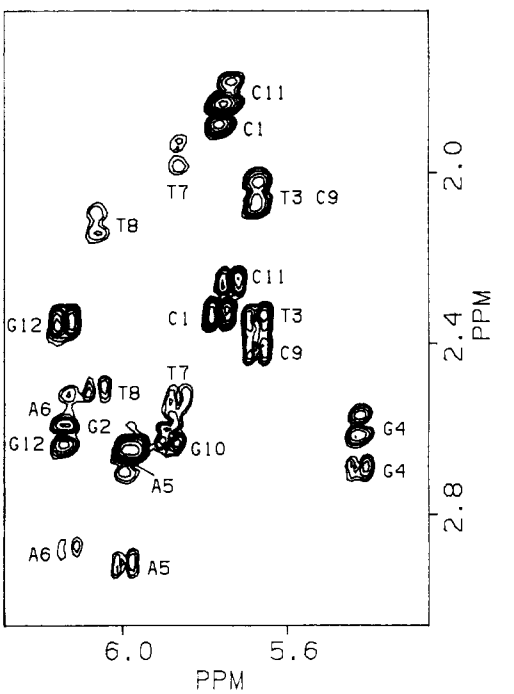

FIGURE 5: Expanded contour plot of the magnitude COSY spectrum of the O^{6}meG·T 12-mer at 25 °C establishing connectivities between the sugar H1′ protons (5.2–6.4 ppm) and the sugar H2′ and H2″ protons (1.7–3.0 ppm). The sugar H2′ and H2″ assignments are designated next to the contour peaks. The H2′ and H2″ protons exhibit different cross-peak patterns due to differences in coupling with other sugar protons.

the purine H8 and pyrimidine H5/CH_3 protons in the purine(3′–5′)pyrimidine G2–T3 step, A6–T7 step, and O^{6}meG10–C11 step (peak A, Figure 4), and NOEs are observed between pyrimidine H6 and pyrimidine H5/CH_3 protons in the pyrimidine(3′–5′)pyrimidine T7–T8 step and T8–C9 step (peak B, Figure 4).

Sugar H2′ and H2″ Proton Assignments. The expanded region of the O^{6}meG·T 12-mer COSY spectrum at 25 °C establishing coupling connectivities between the sugar H1′ protons (5.2–6.3 ppm) and the sugar H2′ and H2″ protons (1.7–3.0 ppm) is presented in Figure 5. We assign the sugar H2′ and H2″ protons in the COSY spectrum on the basis of the known sugar H1′ assignments deduced from an analysis of the NOESY spectrum on the O^{6}meG·T 12-mer duplex. The H1′–H2′ and H1′–H2″ cross peaks have characteristic patterns with all sugar H2′ protons resonating at high fields except for terminal G12, where the patterns are reversed, and for G2 and G10, where the H2′ and H2″ protons are superpositioned on each other (Figure 5). These assignments are confirmed by the resolution of the cross peaks about the 1.8–3.0 ppm H2′ and H2″ spectral region in the expanded COSY spectrum of the O^{6}meG·T 12-mer duplex. The O^{6}meG·T 12-mer duplex sugar H2′ and H2″ proton assignments are listed in Table II.

The expanded 250-ms mixing time NOESY contour plot establishing distance connectivities between the base proton (7.0–8.2 ppm) and sugar H2′ and H2″ protons (1.8–3.0 ppm) in the O^{6}meG·T 12-mer duplex exhibits NOEs between the base protons and the H2′ and H2″ protons of their own and 5′-linked sugar residues characteristic of a right-handed helix, and these results confirm the base and sugar H2′ and H2″ proton assignments for the O^{6}meG·T 12-mer duplex listed in Table II.

Sugar H3′ and H4′ Proton Assignments. We have been unable to unambiguously trace the known H2′ and H2″ assignments (1.8–3.0 ppm) to their H3′ (4.6–5.1 ppm) and in turn to their H4′ (3.6–4.5 ppm) protons due to poor resolution in the H3′ proton spectral region in the O^{6}meG·T 12-mer spectrum. We can make a few H3′ and H4′ assignments with certainty on the basis of an analysis of the COSY and NOESY spectra of the O^{6}meG·T 12-mer duplex, but these are not listed in Table II at this time.

O^{6}meG Base Proton NOEs. We have taken a one-dimensional slice through the 7.97 ppm H8 proton of O^{6}meG10 in

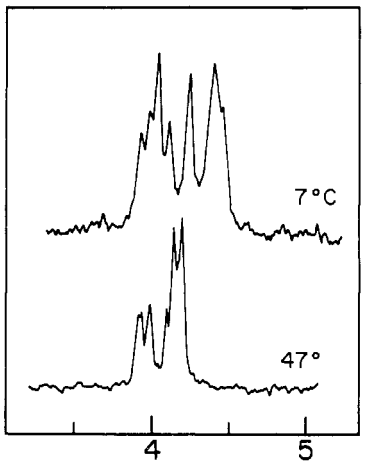

FIGURE 6: Proton noise-decoupled 81-MHz phosphorus NMR spectra of the O^{6}meG·T 12-mer duplex in 0.1 M NaCl, 10 mM phosphate, 1 mM EDTA, and D_2O as a function of temperature between 7 and 47 °C. Chemical shifts are corrected for the temperature dependence of internal standard trimethyl phosphate.

the NOESY spectrum of the O^{6}meG·T 12-mer in the H1′ and H3′ (4.4–6.2 ppm) and the H2′ and H2″ (1.8–3.0 ppm) spectral region. The H8 of O^{6}meG10 exhibits NOEs to the H1′, H3′, H2′, and H2″ of its own sugar, which are stronger than NOEs to the H1′, H2′, and H2″ of its 5′-linked C9 sugar. We also observe the NOE between the H8 of O^{6}meG10 and the H5 of C11 in the O^{6}meG10–C11 step.

We have also taken a one-dimensional slice through the 3.74 ppm OCH_3 protons of O^{6}meG10 in the NOESY spectrum of the O^{6}meG·T 12-mer in the 5.5–8.5 ppm and the 1.0–2.0 ppm spectral regions. The OCH_3 protons of O^{6}meG10 exhibit weak NOEs in the base and sugar H1′ regions with the strongest of these being to that of the H5 proton of the C9 residue. We also observe NOEs between the OCH_3 of O^{6}meG10 and the three thymine CH_3 groups in the O^{6}meG·T 12-mer with the strongest of these being to the CH_3 of the T3 residue.

Phosphodiester Backbone. The proton-decoupled phosphorus spectra of the O^{6}meG·T 12-mer in 0.1 M NaCl between 7 and 47 °C are shown in Figure 6. The phosphorus resonances are partially resolved over a 0.5 ppm spectral dispersion, and no resonances are detected to low and high field of the 4.0–4.5 ppm spectral range.

DISCUSSION

Watson–Crick Imino Protons. We have assigned the five imino protons from the Watson–Crick base pairs (12.3–13.9 ppm) and one imino proton from the T3·O^{6}meG10 modification site (9.05 ppm) from one-dimensional NOEs between protons on the same and adjacent base pairs in the O^{6}meG·T 12-mer duplex in 0.1 M NaCl, pH 6.8 at −5 °C (Figure 1). The chemical shifts are listed in Table I and demonstrate that the G2·C11 and G4·C9 base pairs flanking the T3·O^{6}meG10 interaction are stable in the O^{6}meG·T 12-mer duplex at low temperature.

We do not detect NOEs between the imino protons of G2·C11 and G4·C9 (Figure 1B,C), indicating that T3·O^{6}meG10 acts as a spacer between these two Watson–Crick base pairs in the O^{6}meG·T 12-mer duplex. We have compared the imino proton chemical shifts at the G2·C11 and G4·C9 base pairs flanking the G·T mismatch site in the G·T 12-mer duplex (Patel et al., 1982b) and the O^{6}meG·T modification site in the O^{6}meG·T 12-mer duplex (Table I) at −5 °C. The imino proton of G2·C11 shifts upfield from 13.21 to 12.93 ppm while that of G4·C9 undergoes a larger upfield shift from 12.97 to 12.30 ppm on proceeding from the G·T 12-mer to the

Table III: Comparison of Exchangeable Imino (−5 °C) and Nonexchangeable Base (25 °C) Proton Chemical Shifts in the G·T 12-mer and the O^{6}meG·T 12-mer Duplexes in 0.1 M Salt at 25 °C

		chemical shift (ppm)	
base pair	proton	G·T 12-mer	O^{6}meG·T 12-mer
G2·C11	G H1	*13.21*	*12.93*
	G H8	7.83–7.93	7.89
	C H5	5.42	5.31
	C H6	7.27	7.29
G4·C9	G H1	*12.97*	*12.30*
	G H8	7.83–7.93	7.81
	C H5	5.70	5.63
	C H6	7.51	7.46
T3·*G10[a]	T H3	*11.78*	*9.05*
	*G H8	7.83–7.93	7.97
	T H6	7.18	7.21
	T CH_3	1.70	1.65

[a] *G10 signifies G in the G·T 12-mer and O^{6}meG in the O^{6}meG·T 12-mer.

O^{6}meG·T 12-mer at −5 °C (Table III). The variations could reflect in part differences in stacking between the G·T mismatch on the one hand and the O^{6}meG·T interaction on the other and their flanking base pairs.

The imino protons of the G4·C9, A5·T8, and A6·T7 base pairs broaden simultaneously in the G·T 12-mer duplex (Patel et al., 1982b) and the O^{6}meG·T 12-mer duplex (Figure 2A) on raising the temperature with these protons broadening out at a somewhat lower temperature (by ~7 °C) in the latter duplex. This result supports optical melting studies that demonstrate that the O^{6}meG·T 12-mer duplex exhibits a transition midpoint that is 9 °C lower than the G·T 12-mer duplex (Gaffney et al., 1984).

T3·O^{6}meG10 Imino Proton. The thymidine imino proton in the T3·O^{6}meG10 interaction is detected at 9.0 ppm in the O^{6}meG·T 12-mer duplex (Figures 1 and 2). We observe NOEs between the imino proton of T3 at the T3·O^{6}meG10 modification site and the imino protons of adjacent G2·C11 and G4·C9 base pairs (Figure 1B–D), demonstrating that T3 stacks into the O^{6}meG·T 12-mer duplex.

The 9.05 ppm chemical shift of the T3 imino proton at the T3·O^{6}meG10 site in the O^{6}meG·T 12-mer is to high field of the 13.5–14.5 ppm Watson–Crick A·T base pair (imino to ring-nitrogen hydrogen bond), to high field of the 11.8 ppm wobble G·T base pair (imino to carbonyl hydrogen bond) in the G·T 12-mer, and to high field of the 11 ppm imino proton of thymidine looped out of the helix in extrahelical 13-mer duplexes. The observed chemical shift of the imino proton of T3 suggests that it is not hydrogen bonded to a ring nitrogen or carbonyl group (such hydrogen bonding would result in downfield shifts) and is stacked into the helix resulting in upfield ring current shifts from adjacent base pairs in the O^{6}meG·T 12-mer duplex.

The imino proton of T3 in the T3·O^{6}meG10 interaction exhibits a temperature-independent chemical shift (Figure 3B) compared to the upfield shifts observed with increasing temperature for the Watson–Crick A·T (Figure 3A) and wobble G·T (Patel et al., 1982b) base pairs. The imino protons of Watson–Crick A·T and wobble G·T base pairs are several ppm to low field of their unpaired chemical shifts, and the observed upfield chemical shifts with temperature reflect the increasing fraction of the unpaired state at high temperature. By contrast, the imino proton of T3 in the T3·O^{6}meG10 interaction exhibits a chemical shift typical of an unpaired stacked base, and hence, its chemical shift is independent of temperature.

Nonexchangeable Proton Assignments. The nonexchangeable base and sugar H1′, H2′, and H2″ protons of the

O^{6}meG·T 12-mer duplex in 0.1 M NaCl at 25 °C listed in Table II were assigned from an analysis of two-dimensional COSY and NOESY data sets. We have not been able to definitively assign the H3′ and H4′ protons due to poor resolution between overlapping peaks in the COSY spectrum of the O^{6}meG·T 12-mer duplex.

We have listed the nonexchangeable base proton chemical shifts at the modification site and flanking G2·C11 and G4·C9 base pairs in the G·T 12-mer and the O^{6}meG·T 12-mer duplexes at 25 °C in Table III. We observe similar chemical shifts between these two duplexes for the nonexchangeable protons, which are located on the periphery of the base pairs (Table III). This contrasts with the large shifts observed for the exchangeable imino protons at and adjacent to the modification site between the two duplexes (Table III). The imino protons are located in the center of the base pairs and are sensitive to changes in base pair overlaps in addition to changes in hydrogen bonding.

Since the G2·C11 and G4·C9 base pairs are common to the G·T 12-mer and the O^{6}meG·T 12-mer, the observed imino proton chemical shift differences must reflect different stacking of these base pairs with adjacent T3·G10 in the G·T 12-mer and T3·O^{6}meG10 in the O^{6}meG·T 12-mer duplexes.

Glycosidic Torsion Angles and Helix Type. The NOEs between the bases (purine H8 and pyrimidine H6) and their own sugar H1′ are much weaker in intensity compared to the NOE between the cytidine H6 and H5 protons (designated by asterisks) in the O^{6}meG·T 12-mer duplex at 25 °C (Figure 4). This permits assignment of anti glycosidic torsion angles at the T3 and O^{6}meG10 residues at the modification site and at all other residues in the O^{6}meG·T 12-mer duplex.

The observed directionality of the NOEs between the base (purine H8 and pyrimidine H6) protons and their own and 5′-linked sugar H1′ (Figure 4) and H2′ and H2″ protons establishes that the O^{6}meG·T 12-mer adopts a right-handed helix in solution. This view is supported by the observed directionality of the NOEs between adjacent base protons in purine H8 (3′–5′) pyrimidine H5/CH$_3$ steps and in pyrimidine H6 (3′–5′) pyrimidine H5/CH$_3$ steps (Figure 4) in the O^{6}meG·T 12-mer duplex.

T3·O^{6}meG10 Modification Site. We can probe for perturbations at the O^{6}meG10 modification site by monitoring NOEs between the H8 of O^{6}meG10 and adjacent base and sugar protons in the O^{6}meG·T 12-mer duplex. We have recorded a one-dimensional slice through the 7.97 ppm H8 proton of O^{6}meG10 and observe stronger NOEs to the H1′, H2′, H2″, and H3′ protons of O^{6}meG10 compared to the same sugar protons of the flanking C-9 residue. This suggests a perturbation at the modification site since the NOEs between the H8 of O^{6}meG10 and the H1′ protons of O^{6}meG10 and C9 should be comparable for an unperturbed helix. The perturbation is not large since we can still monitor the NOE between the H8 of O^{6}meG10 and the H5 of C11 in the O^{6}meG10–C11 step in the O^{6}meG·T 12-mer duplex.

A one-dimensional slice has also been taken through the 3.74 ppm OCH$_3$ group of O^{6}meG10 in the O^{6}meG·T 12-mer duplex at 25 °C. The strongest NOEs are observed between the OCH$_3$ group at O^{6}meG10 and the CH$_3$ of T3 across the base pair and the H5 of the flanking C9 residue on the same strand. These results demonstrate that the O^{6}meG10 base stacks into the helix and its OCH$_3$ group is in the major groove and exhibits NOEs to other major groove protons in the O^{6}meG·T 12-mer duplex.

The phosphorus resonances resonate in the 4.0–4.5 ppm spectral dispersion characteristic of an unperturbed helical backbone for the O^{6}meG·T 12-mer at 7 °C (Figure 6). This suggests that incorporation of the T3·O^{6}meG10 interaction does not result in perturbations in the phosphodiester backbone at the modification site. This contrasts with the phosphorus spectrum of the G·T 12-mer duplex where incorporation of the G·T mismatch results in the phosphorus resonances dispersed over 0.75 ppm with one resonance each to low and high field of the 4.0–4.5 ppm unperturbed spectral dispersion (Patel et al., 1982b).

Chart II

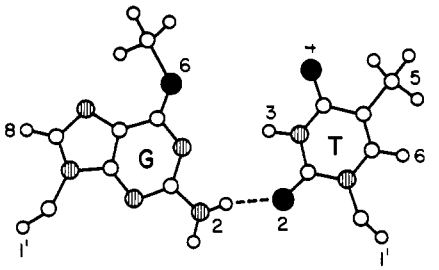

Proposed T3·O^{6}meG10 Pairing. The above results and discussion do not provide direct evidence for the nature of the pairing between the T3 and O^{6}meG10 bases at the modification site in the O^{6}meG·T 12-mer duplex. We note, however, that perturbations from a regular helix are minor on the basis of the observed pattern of base to base NOEs and of base to sugar H1′ NOEs and the unperturbed phosphodiester backbone in the O^{6}meG·T 12-mer duplex. The T3 and O^{6}meG10 bases in the anti conformation can pair through an amino–carbonyl hydrogen bond at the minor groove edge while the bases open out in the major groove edge to avoid unfavorable OCH$_3$–carbonyl interactions (Chart II). The 9.05 ppm upfield chemical shift of the imino proton of T3 suggests that it does not form a normal hydrogen bond to the ring nitrogen of O^{6}meG10 (Chart II), but we cannot eliminate a long hydrogen bond at this time. We propose this pairing scheme for the T3·O^{6}meG10 interaction to stimulate further studies to provide more direct evidence regarding its validity.

O^{6}meG·Pyrimidine 12-mer Duplexes. We compare below the imino proton, nonexchangeable base and sugar protons, and phosphodiester backbone of the O^{6}meG·C 12-mer and O^{6}meG·T 12-mer duplexes.

It is readily apparent that the G2·C11 and G4·C9 base pairs are stable at low temperature when flanked by either the C3·O^{6}meG10 or T3·O^{6}meG10 modification site. We also note that comparable broadening of the imino protons of the central G4·C9, A5·T8, and A6·T7 base pairs occurs at a 5 °C higher temperature in the O^{6}meG·C 12-mer duplex compared to the O^{6}meG·T 12-mer duplex. This ~5 °C stabilization of the C3·O^{6}meG10 interaction relative to the T3·O^{6}meG10 interaction observed by NMR measurements is supported by optical melting experiments where a transition midpoint difference of 7 °C was reported previously (Gaffney et al., 1984).

We compare the chemical shifts of the base and sugar H1′ protons at and adjacent to the modification site in the O^{6}meG·C 12-mer and O^{6}meG·T 12-mer duplexes in Table IV. The largest differences between these two duplexes are detected at the sugar H1′ protons of the G2–C3/T3–G4 segment opposite the C9–O^{6}meG10–C11 segment containing the modification site. We propose that glycosidic torsion angle variations about the anti range are the most likely origin for the large sugar H1′ chemical shift differences at the G2 and T3/C3 positions between the O^{6}meG·C 12-mer and the O^{6}meG·T 12-mer duplexes.

The OCH$_3$ group of O^{6}meG10 resonates at 3.44 and 3.74 ppm in the O^{6}meG·C 12-mer and the O^{6}meG·T 12-mer du-

Table IV: Comparison of the Base Proton Chemical Shifts in the O^6meG·C 12-mer and O^6meG·T 12-mer in 0.1 M NaCl at 25 °C

base pair	proton	O^6meG-C 12-mer	O^6meG·T 12-mer	difference
G2·C11	G H8	7.93	7.89	−0.04
	C H6	7.38	7.29	−0.09
	C H5	5.39	5.31	−0.08
	G H1′	5.55	5.98	*0.43*
	C H1′	5.75	5.75	0.00
C3/T3·O^6meG10	O^6meG H8	8.01	7.97	−0.04
	O^6meG OCH_3	3.44	3.74	0.30
	C/T H6	7.38	7.21	
	C/T H5/CH_3	5.39	1.64	
	O^6meG H1′	5.77	5.89	0.12
	C/T H1′	6.10	5.67	*−0.43*
C4·C9	G H8	7.68	7.81	0.13
	C H6	7.38	7.46	0.08
	C H5	5.58	5.63	0.05
	G H1′	5.29	5.43	0.14
	C H1′	5.52	5.67	0.15

plexes, respectively (Table IV), compared to an unstacked strand value of ~3.95 ppm. This suggests that the OCH_3 group at the modification site stacks better with adjacent base pairs in the O^6meG·C 12-mer compared to the O^6meG·T 12-mer duplex.

A comparison of the phosphorus chemical shift dispersion in the O^6meG·C 12-mer duplex (1.25 ppm dispersion) and the O^6meG·T 12-mer duplex (0.5 ppm dispersion) demonstrates that incorporation of the C3·O^6meG10 interaction perturbs at least three phosphates of the backbone in contrast to the T3·O^6meG10 interaction, which does not appear to perturb the backbone. The conformation of the phosphodiester backbone may be relevant to recognition and correction of mispairing resulting from incorporation of O^6meG into the DNA helix.

It should be noted that the imino protons of the central hexanucleotide core of the standard G·C 12-mer begin to broaden by ~63 °C (Patel et al., 1982) while those of the O^6meG·C 12-mer and O^6meG·T 12-mer begin to broaden by ~45 and ~40 °C, respectively, with the onset of the melting transition in 0.1 M salt solution. Thus, O^6meG incorporation into the duplex results in a destabilization of the entire helix independent of the pyrimidine base opposite the modification site as was independently deduced from optical melting studies (Gaffney et al., 1984).

ACKNOWLEDGMENTS

The two-dimensional NMR spectra were recorded at Northeast Regional NMR Facility WM 500 at Yale University, which is supported by National Science Foundation Grant CHE-7916210. We thank Dr. Dennis Hare for providing access to his two-dimensional NMR processing software and guidance in its usage.

Registry No. O^6meG·T 12-mer, 92984-24-2; O^6meG, 76567-63-0; T, 65-71-4.

REFERENCES

Gaffney, B. L., Marky, L. A., & Jones, R. A. (1984) *Biochemistry 23*, 5686–5691.

Green, C. L., Loechler, E. L., Fowler, K. W., & Essigmann, J. M. (1984) *Proc. Natl. Acad. Sci. U.S.A. 81*, 13–17.

Loechler, E. L., Green, C. L., & Essigmann, J. M. (1984) *Proc. Natl. Acad. Sci. U.S.A. 81*, 6271–6275.

Patel, D. J., Pardi, A., & Itakura, K. (1982a) *Science (Washington, D.C.) 216*, 581–590.

Patel, D. J., Kozlowski, S. A., Marky, L. A., Rice, J. A., Broka, C., Dallas, J., Itakura, K., & Breslauer, K. J. (1982b) *Biochemistry 21*, 437–444.

Patel, D. J., Shapiro, L., Kozlowski, S. A., Gaffney, B. L., & Jones, R. A. (1986) *Biochemistry* (preceding paper in this issue).

Reddy, E. P., Reynolds, R. K., Santos, E., & Barbacid, M. (1983) *Proc. Natl. Acad. Sci. U.S.A. 80*, 4679–4683.

Santos, E., Reddy, E. P., Pulciani, S., Feldman, R. J., & Barbacid, M. (1983) *Proc. Natl. Acad. Sci. U.S.A. 80*, 4679–4683.

Snow, E. T., Foote, R. S., & Mitra, S. (1984) *J. Biol. Chem. 259*, 8095–8100.

Tabin, C. J., Bradley, S. M., Bargmann, C. I., Weinberg, R. A., Papageorge, A. G., Scolnick, E. M., Dhar, R., Lowy, D. R., & Change, E. H. (1982) *Nature (London) 300*, 143–149.

Taparowsky, E., Suard, Y., Fasano, O., Shimizu, K., Goldfarb, M., & Wigler, M. (1982) *Nature (London) 300*, 762–765.